

Quantum Davidson Algorithm for Excited States

Nikolay V. Tkachenko,^{1,3} Yu Zhang,^{2,*} Lukasz Cincio,² Alexander I. Boldyrev,³ Sergei Tretiak,² and Pavel A. Dub^{1,†}

¹*Chemistry Division, Los Alamos National Laboratory, Los Alamos, NM 87545, USA*

²*Theoretical Division, Los Alamos National Laboratory, Los Alamos, NM 87545, USA*

³*Department of Chemistry and Biochemistry, Utah State University, Logan, Utah 84322, USA*

(Dated: April 25, 2022)

Excited states properties are essential for many chemical and physical phenomena, such as charge separation and light emission. However, existing quantum algorithms mainly focus on the ground state, including quantum phase estimation and variational quantum eigensolver (VQE). Even though there are extensions of VQE-type methods for excited states, these methods suffer from optimization problems. Alternatively, the quantum Krylov subspace (QKS) concept has been proposed to calculate ground and excited states, providing a low-cost alternative to quantum phase estimation. However, current QKS methods rely on a pre-generated subspace via real- or imaginary-time evolutions. Such subspace is not compact and may suffer from slow convergence and/or numerical stability problems, resulting in deep circuits. In this work, we develop an economic QKS algorithm, namely the quantum Davidson (QDavidson) algorithm, by leveraging the iterative growth of Krylov subspace and pre-conditioner within the Davidson scheme. The residues of eigenstates are used to expand the Krylov subspace, leading to a compact Krylov subspace close to the exact solutions. Consequently, fast convergence is achieved compared to other QKS methods (e.g., quantum Lanczos). The newly proposed QDavidson algorithm is employed to study the excited-state properties of various systems, including the Heisenberg spin model and real molecules on quantum simulators. Compared to the existing QKS method, the QDavidson algorithm converges fast and results in a much shallower circuit, making QDavidson a practical algorithm for computing both ground and excited states properties on quantum computers.

I. INTRODUCTION

Computing the ground state and excited state properties of many-body systems (especially with strong correlation) is a major challenge in quantum physics and quantum chemistry. The fundamental reason is that the solution space (i.e., the Hilbert space) for the full many-body wave function grows factorially with the system size (e.g., the number of electrons and basis functions) [1–3]. Consequently, many classical quantum chemistry techniques have been developed to avoid the explicit construction of full many-body wavefunctions. Examples include Hartree-Fock (HF) or density functional theory (DFT) theory [4, 5] within which the single-particle picture is used, tensor network methods that optimizes the wave function in the form of a matrix product states [6, 7], selected configuration interaction (sCI) [8, 9] that iteratively expands the configuration interaction (CI) spaces, and coupled-cluster (CC) theory [10] methods. However, these classical techniques are subject to truncation or approximations and are limited to a certain size.

Quantum computers (QC) that leverage the power of collective properties of quantum states have been proposed for simulating quantum mechanics since the 1980s [11]. After four decades of development, quantum computing has entered the Noisy Intermediate-Scale Quantum (NISQ) era [12] and the quantum advantage has been demonstrated on artificial but well-

defined problems [13]. Electronic structure problems, which are essential for many branches of physics, chemistry, and biology, are one of the most promising and immediate applications of quantum computers [1–3, 14]. Many quantum algorithms have been proposed for calculating the ground state of quantum many-body systems on QC since the pioneering work of quantum phase estimation (QPE) [15, 16]. However, due to the noisy nature of NISQ devices, hybrid quantum-classical algorithms with shallower circuits are more NISQ-friendly. Variational quantum eigensolver (VQE) that leverages the power of variational principle was developed accordingly [17]. The VQE scheme deploys the parameterized wavefunction (or ansatz) and the corresponding energy measurement on QCs. Then it variationally minimizes the energy by employing classical optimization algorithms. VQE algorithm has been performed on various quantum architectures such as photons [17], superconducting qubits [18, 19] and trapped ions [20]. Since then, many algorithms have been proposed to further improve the performance or reduce the quantum resource requirements of VQE [21–35].

Despite the extensive development of quantum algorithms for electronic structure problems, most current works focus on the ground state properties. But many novel physical and chemical processes happen on excited states, such as energy transfer [36], bond dissociation [37], and light emission [38]. Hence, it's essential to develop quantum algorithms for excited states. One straightforward way is to extend VQE for excited states by introducing certain constraints [39–47]. Despite the success and impact of VQE algorithms, they suffer from opti-

* zhy@lanl.gov

† pdub@lanl.gov

mization problems. The optimization process in VQE is challenging due to the high nonlinearity of the energy and stochastic errors [48]. And the situation becomes even worse when multiple excited states are included in the optimization.

Alternatively, another emerging direction for calculating excited states on QC is based on quantum subspace, such as Quantum subspace expansion (QSE) based methods [43, 49–52], and non-orthogonal VQE [53]. In addition, the quantum Krylov subspace (QKS) concept has been proposed by leveraging its classical counterpart [54–58]. Current QKS methods apply either real- or imaginary-time [54, 55] evolution to generate the Krylov subspace, which then is used to sample the low-lying spectrum of the Hamiltonian \hat{H} . In particular, Quantum Lanczos (QLanczos) algorithm [55] in a basis of correlated states generated by imaginary-time propagation [59, 60] has been proposed. Even though the QKS methods remove the optimization problems encountered in the VQE algorithms, the current QKS usually requires a deep circuit due to the trotter expansion of the real/imaginary time evolution and a larger number of iterations for convergence. However, the pre-generated Krylov subspace from either real- or imaginary-time evolution is not necessarily compact.

In this work, we propose an economic QKS method, namely Quantum Davidson (QDavidson) algorithm, in which a compact Krylov subspace can be efficiently constructed. The Davidson algorithm leverages the power of the residue and pre-conditioner to confine the search of subspace in the regime close to the exact state, ensuring fast convergence [61]. Compared to its classical counterpart, we developed a strategy to deploy the subspace expansion on the quantum computer without explicit construction of full many-body wave functions on classical computers, leading to the speedup in the subspace projection. Compared to the existing QKS method, the fast convergence of the QDavidson method results in a shallower circuit, making it more noise resilient.

II. THEORY

A. Krylov subspace and classical Davidson algorithm

In the linear algebra, an order- r Krylov subspace generated by a matrix H and a reference vector b is the linear subspace spanned by the images of b under the first r powers of H [62], i.e., $\mathcal{K}_r(H, b) \equiv \{b, Hb, H^2b, \dots, H^{r-1}b\}$. The Krylov subspace has been widely used in numerical algorithms to find the solutions to a high-dimensional matrix, such as the generalized minimal residual method (GMRES), Davidson, and quasi-minimal residual (QMR) algorithms [61].

In quantum chemistry, the iterative Krylov subspace ($\mathcal{K}_r(\hat{H}, |\psi\rangle)$) is particularly useful for finding low-lying states in electronic structure theory. Different ver-

sions of Davidson algorithms have been developed to accelerate the convergence by designing efficient preconditioners [63–65]. The flowchart of the classical Davidson algorithm is presented in Algorithm S1 of the Supplementary Information (SI). Besides, the Davidson algorithm has been generalized to use the non-orthogonal Krylov space [66]. However, the generation of the subspace $\hat{H}^r |\psi\rangle$ is computationally expensive on classical computers when the dimension of \hat{H} becomes large.

B. Quantum Davidson algorithm

In this work, we develop a quantum algorithm counterpart of the Davidson algorithm, namely QDavidson, that leverages the quantum computers to reduce the scaling of generating the Krylov subspace. The QDavidson algorithm utilizes the concept of Krylov subspace and the classical Davidson algorithm to develop an economic QKS algorithm for finding the excited states of the Hamiltonian \hat{H} . Compared to the classical Krylov approach, the QKS scheme uses quantum computers to encode the arbitrarily complex states. Besides, the advantages of QKS methods over the VQE-based techniques are 1) the independent ansatz for each reference state with a compact quantum circuit and 2) the removal of the complicated optimization procedure. In Ref. 55, the quantum imaginary time evolution (QITE) is performed by using Trotter decomposition of the evolution operator ($e^{-\hat{H}t}$) and mapping each Trotter step into unitary. Afterward, the QLanczos algorithm is developed in the Krylov space generated from the snapshots of QITE. However, the QKS generated from the sequential time evolution cannot be compact. Here, we develop the QDavidson algorithm to generate a compact set of QKS, leading to a more economical and numerically stable realization of a QKS method.

Instead of pre-generating the subspace via either real or imaginary-time evolution, QDavidson formalism adaptively grows the QKS by confining the subspace expansion close to the true eigenspace. We employ initially orthogonal states as the reference states. HF ($|\phi_0\rangle$), single-excitation configurations ($|\phi_i^a\rangle = a_a^\dagger a_i |\phi_0\rangle$), and/or configuration-interaction single (CIS) states ($\{\sum_{ia} C_{ia} |\phi_i^a\rangle\}$) are natural choice of initial state. Nevertheless, the set of initial reference states is denoted as ($\{|\psi_k\rangle\}$). Each basis within the Krylov subspace of the j^{th} Davidson iteration takes the following ansatz,

$$|\psi_K\rangle = \hat{U}_K^j \sum_I C_{KI} |\phi_I\rangle \equiv \hat{U}_K^j |\Phi_K\rangle. \quad (1)$$

where the multiple reference states (i.e., a linear combination of HF/CIS states) are used. \hat{U}_K^j are the entanglers determined from the Krylov space expansion, which will be introduced later. $\hat{U}_K^1 = 1$ for the first iteration.

Thus, the general ground and excited states $|\Phi_I\rangle$ can be rewritten as a linear combination of the Krylov vec-

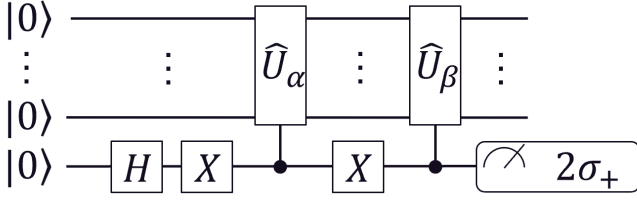


FIG. 1. Schematic diagram of modified Hadamard test for measuring off-diagonal elements. The measurement of the expectation value of $2\sigma_+ = X + iY$ operator.

tors,

$$|\Psi_I\rangle = \sum_K V_{KI} |\psi_K\rangle. \quad (2)$$

Consequently, solving the GS/ES problems ($\hat{H}|\Psi\rangle = E|\Psi\rangle$) can be rewritten as the generalized eigenvalue problem $HV = ESV$ in the Krylov subspace. Where H is the Hamiltonian matrix within the Krylov subspace (Eq. 1), which is defined as

$$H_{KL} = \langle\psi_K|\hat{H}|\psi_L\rangle = \langle\Phi_K|\hat{U}_K^\dagger\hat{H}\hat{U}_L|\Phi_L\rangle. \quad (3)$$

And the overlap matrix element S_{KL} between Krylov vector is

$$S_{KL} = \langle\psi_K|\psi_L\rangle = \langle\Phi_K|\hat{U}_K^\dagger\hat{U}_L|\Phi_L\rangle. \quad (4)$$

These matrix elements of H and S are measured on QC with a ancillary qubit and Hadamard test [53, 54] as demonstrated in Figure 1. Since the dimension of the Krylov subspace is small, the eigenvalue problem $HV = ESV$ can be trivially solved on classical computers.

After the approximate excited-states in the current subspace is solved, the residues of computed states can be obtained

$$|R_I\rangle = \hat{H}|\Psi_I\rangle - E|\Psi_I\rangle = (\hat{H} - E) \sum_K V_{KI} |\psi_K\rangle. \quad (5)$$

The norm of the residue can be readily measured on the quantum computers in a similar manner of H_{KL} measurement,

$$\begin{aligned} ||R_I|| &= \langle\Psi_I|(\hat{H} - E_I)^2|\Psi_I\rangle \\ &= \sum_{KL} V_{KI}^* V_{LI} \langle\psi_K|(\hat{H} - E_I)^2|\psi_L\rangle. \end{aligned} \quad (6)$$

The norm measures the convergence of each eigenstate. If $||R_I||$ is large than ϵ (ϵ is the convergence criteria), a new Krylov vector based on the normalized counterpart of $|R_I\rangle$ should be added within the Davidson algorithm if it has no linear dependence within the current Krylov subspace. The classical Davidson uses the Krylov subspace $\mathcal{K}_r((\hat{H} - E), |\Phi_I\rangle)$ to solve the eigenvalue problem.

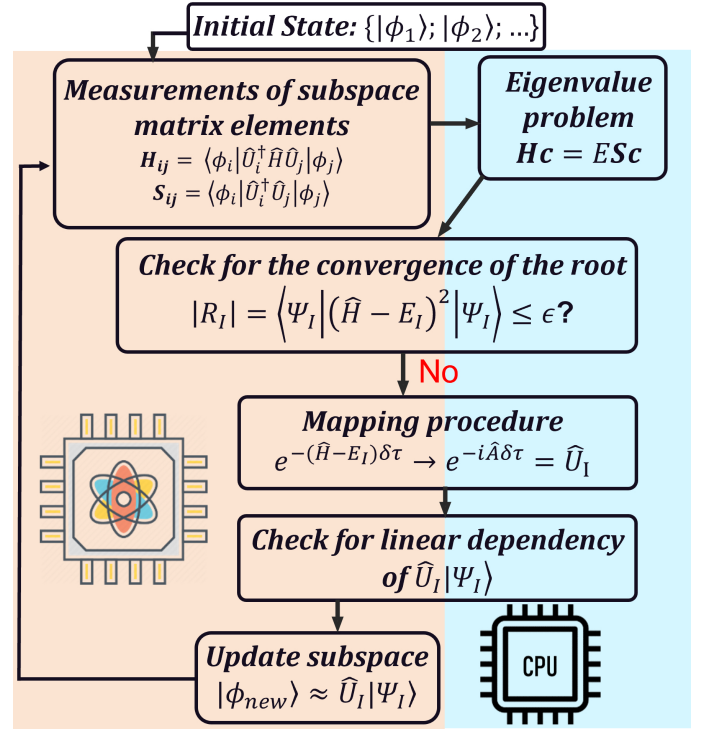


FIG. 2. Flowchart of the QDavidson Algorithm. The orange (blue) box represents the part of the algorithm that is performed on QPU (CPU).

However, it is non-trivial to create the $\hat{H}|\Psi_I\rangle$ state on quantum circuits with the non-unitary \hat{H} . Alternatively, within the QDavidson algorithm, a correction vector defined by

$$|\delta_I\rangle = e^{-\Delta\tau(\hat{H}-E)} |\Psi_I\rangle \quad (7)$$

is used to expand the Krylov subspace, i.e., the QDavidson algorithm uses the subspace of $\mathcal{K}_r(e^{-\Delta\tau(\hat{H}-E)}, |\Phi_I\rangle)$ to find the eigenstates. Because $|\delta_I\rangle = [1 - \Delta\tau(\hat{H} - E)]|\Phi_I\rangle + \mathcal{O}(\Delta\tau)$, it can be verified that $\mathcal{K}_r(e^{-\delta\tau(\hat{H}-E)}, |\Phi_I\rangle)$ is equivalent to $\mathcal{K}_r((\hat{H} - E), |\Phi_I\rangle)$ if $\Delta\tau \rightarrow 0$. The evolution in Equation 7 is then mapped into unitary operators $e^{-i\hat{A}}$ as proposed in Ref. [55], and Eq. 7 can be finally rewritten as

$$|\delta_I\rangle = n_I e^{-i\hat{A}} |\Phi_I\rangle \quad (8)$$

where n_I is the normalization factor. Alternatively, the preconditioned residue $\frac{1}{\hat{H}-E_I}(\hat{H} - E)$ can be directly mapped into $e^{-i\delta\tau\hat{A}}$ by $|\delta_I\rangle = \frac{1}{\hat{H}-E_I}(\hat{H} - E)|\Phi_I\rangle \simeq C e^{-i\hat{A}} |\Phi_I\rangle$. The latter method does not require Trotter decomposition and it can be connected to any other measurement reduction techniques, which may be more measurement-efficient.

After mapping the residue operator into unitaries, the QDavidson algorithm examines whether the new Krylov vectors (or correction vector) have linear-dependence in

current subspace by introducing $|\delta'_{K'}\rangle$

$$\begin{aligned} |\delta'_{I'}\rangle &\equiv |\delta_I\rangle - \sum_{KJ} |\Psi_K\rangle (S^{-1})_{KJ} \langle \Psi_J | \delta_I \rangle \\ &\equiv |\delta_I\rangle - \sum_{KJ} (S^{-1})_{KJ} d_{IJ} |\delta_I\rangle. \end{aligned} \quad (9)$$

Where $d_{KJ} = \langle \Psi_J | \delta_I \rangle$ and the norm $||\delta'_{I'}\rangle||$ are measured on QC. If $\frac{||\delta'_{I'}\rangle||}{||\delta_I\rangle} > \epsilon$, it means that the the Krylov vector cannot be well presented in current subspace (i.e., cannot find linear dependence of $|\delta'_{I'}\rangle$ in current subspace) and $|\delta'_{I'}\rangle$ should be added into the subspace. Since the new Krylov vector added into the Krylov space introduces additional correlations, the new iteration will bring the results closer to the exact solutions. The QDavidson algorithm is summarized in Fig. 2.

C. Complexity of Quantum Davidson algorithm

Since the size of the Krylov subspace (N_K) is small, solving the generalized eigenvalue problems on classical computers is cheap. The major complexity of the QDavidson algorithm comes from the mapping of residue vectors into unitaries. Thus, the main bottleneck of the QDavidson algorithm is the construction of S , b and solving the linear system to get unitary \hat{A} . Previous work found that the mapping of the non-unitary exponential operators into unitaries scales exponentially against correlation domain D [55]. But local approximation can be made to remove the exponential dependence on D [55], resulting in polynomial complexity.

III. NUMERICAL EXPERIMENTS

In this section, we provide numerical results for the proposed algorithm. To demonstrate the performance of the QDavidson algorithm, we carried out an exact quantum simulation of various systems, including one-dimensional (1D) Heisenberg models and molecular systems, using the noiseless state-vector simulator.

A. One dimensional Heisenberg models

The long-range (LR) and short-range (SR) one-dimensional (1D) Heisenberg models analogs to the models described in Ref. [55] were tested in this work. While the short-range models introduce only nearest-neighbor interactions between spins (given by $C_{ij}(\hat{X}_i\hat{X}_j + \hat{Y}_i\hat{Y}_j + \hat{Z}_i\hat{Z}_j)$ terms), the long-range models include pairwise interactions between all spins. They, therefore, include a larger number of terms in a qubit Hamiltonian. Explicitly the long-range and short-range Hamiltonians can be

expressed as the following:

$$\hat{H}_{SR} = - \sum_{i=1}^N \hat{S}_i \hat{S}_{i+1} \quad (10)$$

$$\hat{H}_{LR} = - \sum_{i,j;j>i}^N \frac{1}{D_{ij}} \hat{S}_i \hat{S}_j. \quad (11)$$

Where $D_{ij} = \min(1+|j-i|, 1+N-|j-i|)$. N is the number of spins in the system. For short-range Hamiltonians, the index i is cyclic, i.e., reaching the value of $N+1$ index will jump to the value 1. The QDavidson algorithm is state-dependent. Thus the initial state must be defined. The algorithm was initiated with the anti-ferromagnetic product state, which corresponds to an alternating $|01\dots\rangle$ state on a computational basis. To compare the results of the QDavidson algorithm with other QKS methods, we also performed a QLanczos algorithm with identical initial parameters.

The results of QDavidson and QLanczos algorithms for the 1D-Heisenberg models are shown in Figure 3. As we can see, for the first four low-lying solutions, the convergence of the QDavidson algorithm can be achieved within 4 and 7 iterations for 4-spin and 6-spin systems, respectively (Figure 3e-h). This result outperforms the recently proposed QLanczos [55] algorithm (Figure 3a-d), which suffers not only from slow convergence but also from numerical instability since the produced states rapidly become linearly dependent. With the introduction of the root convergence criteria and the linear dependency check, the QDavidson algorithm is more numerically stable. The complete results for the QLanczos algorithm are given in the Supplementary Information (SI) (Figure S1). The algorithm was performed until the iteration at which a linearly dependent state was obtained. We note that QLanczos was able to achieve the exact values of energies for all 4 spin models within 6 iterations (Figure S1a-b). However, for 6-spin systems, the convergence was not achieved, and the final energy values were found with a significant error (Figure S1c-d).

Since a new entangler is appended after mapping the imaginary time evolution operator into unitaries, the circuit depth increases monotonically with iterations within the QITE, QLanczos, and QDavidson frameworks. Consequently, faster convergence leads to shallower circuits. Compared to the QITE algorithms, QLanczos converges faster in finding the ground state [55]. Our QDavidson algorithm significantly improves the convergence by using the residue operator to confine the search of subspace in the regime close to the exact state, resulting in a much shallower circuit depth.

B. π -conjugated hydrocarbons

Besides the 1D Heisenberg models, we also tested our algorithm on chemical systems. Predictably, molecular

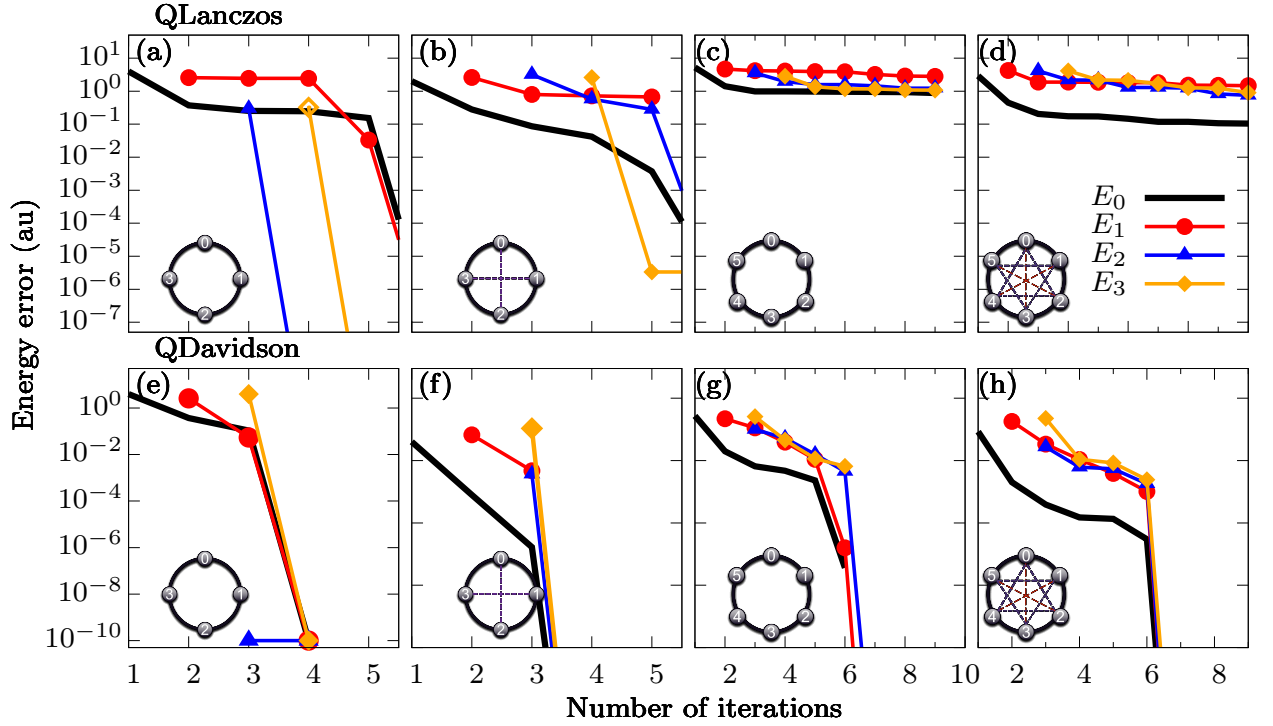


FIG. 3. Energy differences of the 1D Heisenberg as function of algorithm iteration. The energy difference is defined as $E_{\text{algorithm}} - E_{\text{exact}}$. Results for different states are given with different colors: black - ground state; blue - first excited state; green; second excited state; red - third excited state. Graphs a-d show the result of the QLanczos algorithm, while graphs e-h show the results of the QDavidson algorithm obtained with the same QITE expansion parameters. Graphical representations of each system are given in the left bottom corner of each graph. The small circles with numbers represent spins, while lines connecting those circles represent $C_k \hat{S}_i \hat{S}_j$ terms. Different C_k coefficients are illustrated with lines of different colors and widths.

Hamiltonians are much more complicated than the 1D-Heisenberg models since they include nontrivial entanglement between multiple orbitals. To prove the advantage of the QDavidson algorithm for molecular systems, we consider three molecular systems: ethylene, cyclopropene cation, and benzene. Cartesian coordinates of the investigated molecular systems are given in the SI (Table S1). An active space representing the π -conjugated system has been chosen for all systems. The explicit active orbitals shapes are given in the SI (Figure S2). Thus, the (2e, 2o) active space was considered for C_2H_4 molecule, (2e, 3o) for $C_3H_3^+$, and (6e, 6o) for C_6H_6 . The Jordan-Wigner transformation [67] was used to convert the second-quantized Hamiltonian into qubit Hamiltonian. Thus the largest system considered in this study is the benzene molecule, which includes 6 electrons and 12 spin-orbitals in the active space (which corresponds to a 12-qubit Hamiltonian with 407 terms).

Since the electronic structure problems in molecular systems possess particle preserving and total spin preserving symmetries, it is helpful to define a more symmetric pool of Pauli-terms that will be used in correction vector $|\delta_I\rangle$ mapping. Thus, a set of all possible spin projection preserving single and double excitation operators was chosen and then transformed into qubit operators

using the Jordan-Wigner [67] scheme. All unique Pauli-terms with the odd number of \hat{Y} operators were then added into the pool. Thus the pool includes 12 terms for ethylene molecule, 40 terms for cyclopropene cation, and 828 unique Pauli-terms for benzene.

The performance of the QDavidson algorithm depends on the initial state that was defined. Several simulations were performed with different initial configurations ($|\phi_0\rangle, |\phi_i^a\rangle = a_a^\dagger a_i |\phi_0\rangle$). In particular, the Hartree-Fock, the first excited singlet, and the first triplet product states were considered. The QDavidson algorithm converges to exact energy values for the smallest molecular systems within several iterations. Thus, for C_2H_4 , starting from the Hartree-Fock product state QDavidson algorithm was able to find the exact ground state energy (-77.11518 Hartree) and exact second excited singlet state energy (-76.37541 Hartree) after one iteration. Similar results were obtained for the $C_3H_3^+$ system, where the exact ground state (-113.64929 Hartree) and exact first three singlet excited states were located. Results for other initial states are shown in Table I. Interestingly, the eigenstates that were found for the $C_3H_3^+$ system are particle preserving and do not fall into a neutral state solution with 3 electrons instead of two (although they are lower in energy).

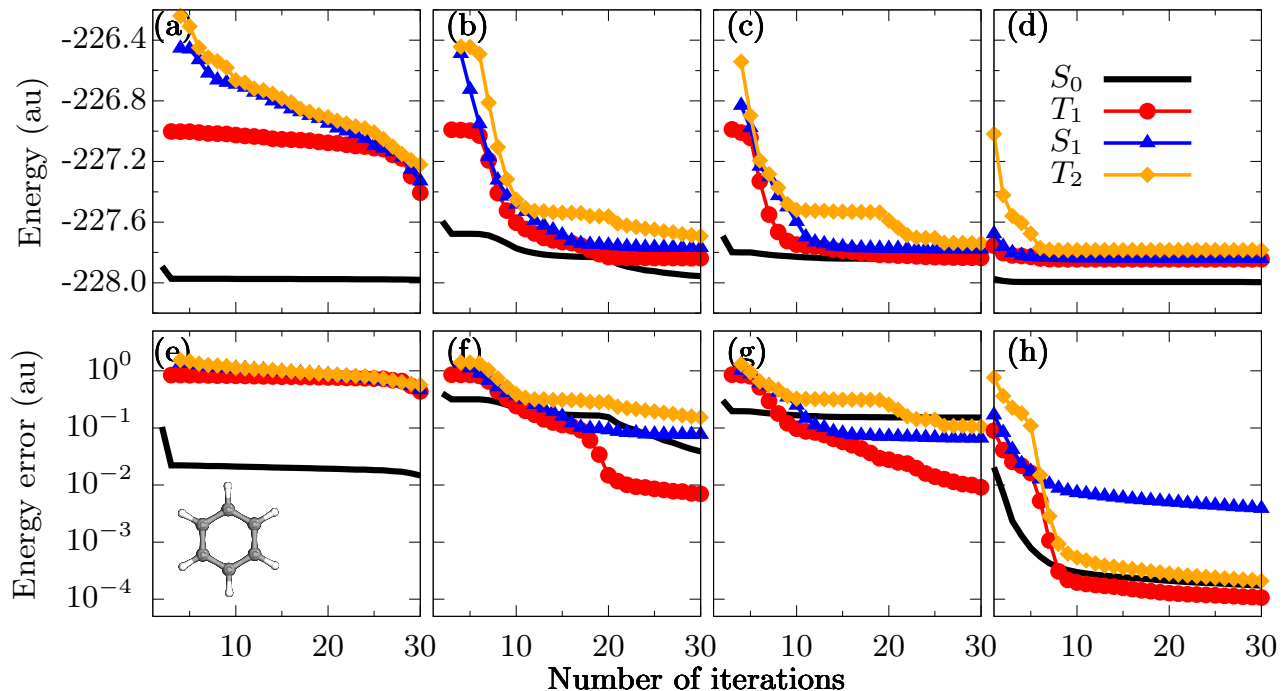


FIG. 4. Energies and errors of the first four low-lying states (S_0 , T_1 , S_1 , T_2) obtained from the QDavidson procedure as a function of algorithm iteration. Results for different states are given in different colors. The results for C_6H_6 molecule initialised with different product states: $|000000111111\rangle$ (a, e); $|000010011111\rangle$ (b, f); $|000001011111\rangle$ (c, g); combination of three product states mentioned above (d, h). Black dashed horizontal lines show the exact energies obtained from a direct diagonalization of the corresponding Hamiltonian. The geometry of the molecule is shown in the inset of (e).

For the more extensive C_6H_6 system, the QDavidson algorithm also located the energy of several low-lying states within chemical accuracy. However, a significantly larger number of iterations are required (Figure 4a-c). Presumably, this is due to the limited operator pool that was chosen. Since it includes only Pauli words from JW-mapped single and double excitation operators, multiple electron systems (number of electrons greater than 2) may suffer from not sufficient flexibility in $e^{-\Delta\tau(\hat{H}-E)}$ operator mapping. Nevertheless, the algorithm could obtain meaningful results even with the restricted operator pool. Thus, for the benzene molecule, the algorithm was able to find the first excited singlet and triplet states within 10^{-2} Hartree after about 30 iterations (Figure 4b, c).

For a larger system, we can vividly observe that starting the algorithm from the single initial state is not the best strategy to obtain the first several low-lying excited states (Figure 4a-c). Although the algorithm could locate states of interest, the accuracy is far from the desired precision of 10^{-3} Hartree. Even initiating the algorithm with the first excited singlet (Figure 4f) or triplet (Figure 4g) determinants leads to faster convergence in comparison to HF initial state, the energies are still converging slowly, and far from the exact values. In turn, generalization of the algorithm with the multiple initial states leads to faster convergence and more precise results (Fig-

ure 4h), highlighting the importance of multireference states. In particular, the chemically accurate energies of S_0 , T_1 , and T_2 states could be obtained after 11 iterations. Thus, to locate the low lying excited states for a large molecular system, one should start with multiple initial states to speed up the energy convergence.

IV. SUMMARY

In this work, we developed an efficient QKS algorithm, namely QDavidson, for computing ground states and low-lying excited states by leveraging the power of the Krylov subspace and fast convergence of the Davidson algorithm. In contrast to other QKS methods that use the real or imaginary time to pre-generate a subspace, the QDavidson algorithm uses the residues of approximated states obtained from the previous iteration to grow the subspace. The Davidson algorithm leverages the power of the pre-conditioner to confine the search of subspace in the regime close to the exact state, ensuring fast convergence. Our Numerical simulations confirm that the QDavidson algorithm converges much faster than other QKS methods. Since the circuit depth increases with iterations, the fast convergence of the QDavidson algorithm results in shallower quantum circuits, making it more noise resilient. In the future, we will explore other

Molecule	Initial state	Number of iterations	Energies
C_2H_4	0011⟩	1	-77.11518 (S_0), $S_z = 0$ -76.37541 (S_2), $S_z = 0$
	1001⟩	1	-76.92218 (T_1), $S_z = 0$ -76.58276 (S_1), $S_z = 0$
	0101⟩	0 ^a	-76.92218 (T_1), $S_z = 1$
$C_3H_3^+$	000011⟩	2	-113.64929 (S_0), $S_z = 0$ -113.19854 (S_1), $S_z = 0$ -112.75964 (S_2), $S_z = 0$ -112.68141 (S_3), $S_z = 0$
	001001⟩	2	-113.35209 (T_1), $S_z = 0$ -113.19854 (S_1), $S_z = 0$ -112.96818 (T_2), $S_z = 0$ -112.75964 (S_2), $S_z = 0$
	000101⟩	0 ^a	-113.35209 (T_1), $S_z = 1$

^a The initial product state is already an exact solution.

TABLE I. Results of QDavidson algorithm for C_2H_4 and $C_3H_3^+$ molecules. The initial state and number of iterations for the algorithm convergence are given. Different eigenstates are denoted in parenthesis as the following: S_0 - ground singlet state, T_1 - the lowest triplet state, S_i - i^{th} excited singlet state, T_i - i^{th} excited triplet state. The S_z denotes spin projection of the obtained state.

advanced pre-conditioner for Davidson method [63, 65], which could further reduce the iterative steps and circuit depth in return. In addition, the accuracy of the simulation is limited by choice of basis set. In principle, a large basis set is required to achieve chemical accuracy. However, increasing the basis set size in quantum algorithms is not NISQ friendly, which requires a significantly larger

number of qubits and deeper circuits [68]. Alternatively, by using a trans-correlated Hamiltonian, one can achieve the accuracy at the cc-pVTZ basis even with a minimal basis set [68], which will be explored in our future work.

ACKNOWLEDGMENTS

The research presented in this article was supported by the Laboratory Directed Research and Development (LDRD) program of Los Alamos National Laboratory (LANL) under project number 20200056DR. We thank LANL Institutional Computing (IC) program for access to HPC resources. S.T. acknowledges the support from the center of integrated nanotechnologies (CINT), a U.S. Department of Energy and Office of Basic Energy Sciences User Facility. LANL is operated by Triad National Security, LLC, for the National Nuclear Security Administration of the U.S. Department of Energy (contract no. 89233218CNA000001). A.I.B. and N.V.T. acknowledge funding from the subcontract with LANL (Award ID: 203369-00001). A.I.B. acknowledges financial support from the R. Gaurth Hansen Professorship fund.

Data availability

The data that support the findings of this study are available from the corresponding authors on reasonable request.

Code availability

The code used to generate the data presented in this study is available from the corresponding authors on reasonable request.

-
- [1] Y. Cao, J. Romero, J. P. Olson, M. Degroote, P. D. Johnson, M. Kieferová, I. D. Kivlichan, T. Menke, B. Peropadre, N. P. Sawaya, *et al.*, **Chem. Rev.** **119**, 10856 (2019).
- [2] S. McArdle, S. Endo, A. Aspuru-Guzik, S. C. Benjamin, and X. Yuan, **Rev. Mod. Phys.** **92**, 015003 (2020).
- [3] B. Bauer, S. Bravyi, M. Motta, and G. K.-L. Chan, **Chem. Rev.** **120**, 12685 (2020).
- [4] A. J. Cohen, P. Mori-Sánchez, and W. Yang, **Chem. Rev.** **112**, 289 (2012).
- [5] N. Schuch and F. Verstraete, **Nat. Phys.** **5**, 732 (2009).
- [6] G. K.-L. Chan and S. Sharma, **Ann. Rev. Phys. Chem.** **62**, 465 (2011).
- [7] U. Schollwöck, **Ann. Phys.** **326**, 96 (2011), january 2011 Special Issue.
- [8] N. M. Tubman, C. D. Freeman, D. S. Levine, D. Hait, M. Head-Gordon, and K. B. Whaley, **J. Chem. Theory Comput.** **16**, 2139 (2020).
- [9] M. Dash, J. Feldt, S. Moroni, A. Scemama, and C. Filippi, **J. Chem. Theory Comput.** **15**, 4896 (2019).
- [10] D. I. Lyakh, M. Musiał, V. F. Lotrich, and R. J. Bartlett, **Chem. Rev.** **112**, 182 (2012).
- [11] R. P. Feynman, **Int. J. Theor. Phys.** **21**, 467 (1982).
- [12] J. Preskill, **Quantum** **2**, 79 (2018).
- [13] F. Arute, K. Arya, R. Babbush, D. Bacon, J. C. Bardin, R. Barends, R. Biswas, S. Boixo, F. G. S. L. Brandao, D. A. Buell, B. Burkett, Y. Chen, Z. Chen, B. Chiaro, R. Collins, W. Courtney, A. Dunsworth, E. Farhi, B. Foxen, A. Fowler, C. Gidney, M. Giustina, R. Graff, K. Guerin, S. Habegger, M. P. Harrigan, M. J. Hartmann, A. Ho, M. Hoffmann, T. Huang, T. S. Humble, S. V. Isakov, E. Jeffrey, Z. Jiang, D. Kafri, K. Kechedzhi, J. Kelly, P. V. Klimov, S. Knysh, A. Korotkov, F. Kostritsa, D. Landhuis, M. Lindmark, E. Lucero, D. Lyakh, S. Mandrà, J. R. McClean, M. McEwen, A. Megrant, X. Mi, K. Michielsen, M. Mohseni, J. Mutus, O. Naaman, M. Neeley, C. Neill, M. Y. Niu, E. Ostby, A. Petukhov, J. C. Platt, C. Quintana, E. G. Rieffel, P. Roushan, N. C. Rubin, D. Sank, K. J. Satzinger, V. Smelyanskiy, K. J. Sung, M. D. Trevithick, A. Vainsencher, B. Villalonga, T. White, Z. J. Yao, P. Yeh, A. Zalcman, H. Neven, and J. M. Martinis, **Nature** **574**, 505 (2019).
- [14] Y. Alexeev, D. Bacon, K. R. Brown, R. Calderbank, L. D. Carr, F. T. Chong, B. DeMarco, D. Englund, E. Farhi, B. Fefferman, A. V. Gorshkov, A. Houck, J. Kim, S. Kimmel, M. Lange, S. Lloyd, M. D. Lukin, D. Maslov, P. Maunz, C. Monroe, J. Preskill, M. Roetteler, M. J. Savage, and J. Thompson, **PRX Quantum** **2**, 017001 (2021).

- [15] D. S. Abrams and S. Lloyd, *Phys. Rev. Lett.* **83**, 5162 (1999).
- [16] A. Kitaev, A. Shen, M. Vyalii, and M. Vyalii, *Classical and Quantum Computation*, Graduate studies in mathematics (American Mathematical Society, 2002).
- [17] A. Peruzzo, J. McClean, P. Shadbolt, M. H. Yung, X. Q. Zhou, P. J. Love, A. Aspuru-Guzik, and J. L. O’Brien, *Nat. Commun.* **5**, 4213 (2014).
- [18] A. Kandala, K. Temme, A. D. Córcoles, A. Mezzacapo, J. M. Chow, and J. M. Gambetta, *Nature* **567**, 491 (2019).
- [19] A. Kandala, A. Mezzacapo, K. Temme, M. Takita, M. Brink, J. M. Chow, and J. M. Gambetta, *Nature* **549**, 242 (2017).
- [20] Y. Nam, J.-S. Chen, N. C. Pienti, K. Wright, C. Delaney, D. Maslov, K. R. Brown, S. Allen, J. M. Amini, J. Apisdorf, K. M. Beck, A. Blinov, V. Chaplin, M. Chmielewski, C. Collins, S. Debnath, K. M. Hudek, A. M. Ducore, M. Keesan, S. M. Kreikemeier, J. Mizrahi, P. Solomon, M. Williams, J. D. Wong-Campos, D. Moehring, C. Monroe, and J. Kim, *npj Quantum Inf.* **6**, 33 (2020).
- [21] N. V. Tkachenko, J. Sud, Y. Zhang, S. Tretiak, P. M. Anisimov, A. T. Arrasmith, P. J. Coles, L. Cincio, and P. A. Dub, *PRX Quantum* **2**, 020337 (2021).
- [22] I. G. Ryabinkin, R. A. Lang, S. N. Genin, and A. F. Izmaylov, *J. Chem. Theory Comput.* **16**, 1055 (2020).
- [23] H. R. Grimsley, S. E. Economou, E. Barnes, and N. J. Mayhall, *Nat. Commun.* **10**, 3007 (2019).
- [24] Y. Zhang, L. Cincio, C. F. A. Negre, P. Czarnik, P. Coles, P. M. Anisimov, S. M. Mniszewski, S. Tretiak, and P. A. Dub, arXiv preprint arXiv:2106.07619.
- [25] H. L. Tang, V. Shkolnikov, G. S. Barron, H. R. Grimsley, N. J. Mayhall, E. Barnes, and S. E. Economou, *PRX Quantum* **2**, 020310 (2021).
- [26] I. G. Ryabinkin, A. F. Izmaylov, and S. N. Genin, *Quantum Sci. Tech.* **6**, 024012 (2021).
- [27] R. A. Lang, I. G. Ryabinkin, and A. F. Izmaylov, *J. Chem. Theory Comput.* **17**, 66 (2021).
- [28] Z.-J. Zhang, T. H. Kyaw, J. Kottmann, M. Degroote, and A. Aspuru-Guzik, *Quantum Sci. Tech.* (2021).
- [29] H. R. Grimsley, S. E. Economou, E. Barnes, and N. J. Mayhall, *Nat. Commun.* **10**, 3007 (2019).
- [30] R. A. Lang, I. G. Ryabinkin, and A. F. Izmaylov, *J. Chem. Theory Comput.* **17**, 66 (2021).
- [31] Y. S. Yordanov, V. Armaos, C. H. W. Barnes, and D. R. M. Arvidsson-Shukur, “Iterative qubit-excitation based variational quantum eigensolver,” (2020), arXiv:2011.10540.
- [32] X. Yuan, J. Sun, J. Liu, Q. Zhao, and Y. Zhou, arXiv:2007.00958 (2021).
- [33] A. Gu, A. Lowe, P. A. Dub, P. J. Coles, and A. Arrasmith, arXiv e-prints, arXiv:2108.10434 (2021), arXiv:2108.10434.
- [34] M. Cerezo, A. Arrasmith, R. Babbush, S. C. Benjamin, S. Endo, K. Fujii, J. R. McClean, K. Mitarai, X. Yuan, L. Cincio, and P. J. Coles, *Nat. Rev. Phys.* **3**, 625 (2021).
- [35] K. Bharti, A. Cervera-Lierta, T. H. Kyaw, T. Haug, S. Alperin-Lea, A. Anand, M. Degroote, H. Heimonen, J. S. Kottmann, T. Menke, W.-K. Mok, S. Sim, L.-C. Kwek, and A. Aspuru-Guzik, “Noisy intermediate-scale quantum (nisq) algorithms,” (2021), arXiv:2101.08448.
- [36] T. R. Nelson, D. Ondarse-Alvarez, N. Oldani, B. Rodriguez-Hernandez, L. Alfonso-Hernandez, J. F. Galindo, V. D. Kleiman, S. Fernandez-Alberti, A. E. Roitberg, and S. Tretiak, *Nat. Commun.* **9**, 2316 (2018).
- [37] Y. Zhang, L. Li, S. Tretiak, and T. Nelson, *J. Chem. Theory Comput.* **16**, 2053 (2020).
- [38] T. R. Nelson, A. J. White, J. A. Bjorgaard, A. E. Sifain, Y. Zhang, B. Nebgen, S. Fernandez-Alberti, D. Mozyrsky, A. E. Roitberg, and S. Tretiak, *Chem. Rev.* **120**, 2215 (2020).
- [39] K. M. Nakanishi, K. Mitarai, and K. Fujii, *Phys. Rev. Research* **1**, 033062 (2019).
- [40] O. Higgott, D. C. Wang, and S. Brierley, *Quantum* **3**, 1 (2019).
- [41] R. M. Parrish, E. G. Hohenstein, P. L. McMahon, and T. J. Martínez, *Phys. Rev. Lett.* **122**, 230401 (2019).
- [42] Y. Shen, X. Zhang, S. Zhang, J.-N. Zhang, M.-H. Yung, and K. Kim, *Phys. Rev. A* **95**, 020501 (2017).
- [43] J. R. McClean, M. E. Kimchi-Schwartz, J. Carter, and W. A. de Jong, *Phys. Rev. A* **95**, 042308 (2017).
- [44] K. M. Nakanishi, K. Mitarai, and K. Fujii, *Phys. Rev. Research* **1**, 033062 (2019).
- [45] O. Higgott, D. Wang, and S. Brierley, *Quantum* **3**, 156 (2019).
- [46] H. Kawai and Y. O. Nakagawa, *Mach. Learn.: Sci. Technol.* **1**, 045027 (2020).
- [47] G. Greene-Diniz and D. Muñoz Ramo, *Int. J. Quantum Chem.* **121**, e26352 (2021).
- [48] D. Stilck França and R. García-Patrón, *Nat. Phys.* **17**, 1221 (2021).
- [49] J. I. Colless, V. V. Ramasesh, D. Dahlen, M. S. Blok, M. E. Kimchi-Schwartz, J. R. McClean, J. Carter, W. A. de Jong, and I. Siddiqi, *Phys. Rev. X* **8**, 011021 (2018).
- [50] T. Takeshita, N. C. Rubin, Z. Jiang, E. Lee, R. Babbush, and J. R. McClean, *Phys. Rev. X* **10**, 011004 (2020).
- [51] R. M. Parrish and P. L. McMahon, arXiv:1909.08925.
- [52] P. J. Ollitrault, A. Kandala, C.-F. Chen, P. K. Barkoutsos, A. Mezzacapo, M. Pistoia, S. Sheldon, S. Woerner, J. M. Gambetta, and I. Tavernelli, *Phys. Rev. Research* **2**, 043140 (2020).
- [53] W. J. Huggins, J. Lee, U. Baek, B. O’Gorman, and K. B. Whaley, *New J. Phys.* **22**, 073009 (2020).
- [54] N. H. Stair, R. Huang, and F. A. Evangelista, *J. Chem. Theory Comput.* **16**, 2236 (2020).
- [55] M. Motta, C. Sun, A. T. K. Tan, M. J. O’Rourke, E. Ye, A. J. Minnich, F. G. S. L. Brandão, and G. K.-L. Chan, *Nat. Phys.* **16**, 205 (2020).
- [56] C. L. Cortes and S. K. Gray, *Phys. Rev. A* **105**, 022417 (2022).
- [57] K. Yeter-Aydeniz, B. T. Gard, J. Jakowski, S. Majumder, G. S. Barron, G. Siopsis, T. Humble, and R. C. Pooser, arXiv:2102.05511 (2021).
- [58] E. N. Epperly, L. Lin, and Y. Nakatsukasa, arXiv:2110.07492 (2021).
- [59] S. McArdle, T. Jones, S. Endo, Y. Li, S. C. Benjamin, and X. Yuan, *npj Quantum Info.* **5**, 75 (2019).
- [60] K. Yeter-Aydeniz, R. C. Pooser, and G. Siopsis, *npj Quantum Inf.* **6** (2020).
- [61] Y. Saad, *Iterative Methods for Sparse Linear Systems*, 2nd ed., Other Titles in Applied Mathematics (SIAM, 2003).
- [62] C. Lanczos, *J. Res. Natl. Bur. Stand. B* **45**, 255 (1950).
- [63] R. M. Parrish, E. G. Hohenstein, and T. J. Martínez, *J. Chem. Theory Comput.* **12**, 3003 (2016).
- [64] S. Tretiak, C. M. Isborn, A. M. N. Niklasson, and M. Challacombe, *J. Chem. Phys.* **130**, 054111 (2009).
- [65] Z. Zhou and S. M. Parker, *J. Chem. Phys.* **155**, 204111 (2021).

- (2021).
- [66] F. Furche, B. T. Krull, B. D. Nguyen, and J. Kwon, *J. Chem. Phys.* **144**, 174105 (2016).
- [67] P. Jordan and E. Wigner, *Zeitschrift für Physik* **47**, 631 (1928).
- [68] A. Kumar, A. Asthana, C. Masteran, E. F. Valeev, Y. Zhang, L. Cincio, S. Tretiak, and P. A. Dub, arXiv:2201.09852 (2022).

Supplementary Information for “Quantum Davidson Algorithm for Excited States”

Appendix A: Mapping Residue into unitaries

In this appendix, we discuss the way of mapping residue in Davidson algorithm, $(\hat{H} - E_i)|\Phi_i\rangle$, into unitaries $e^{-i\hat{A}}\Phi_i$ on quantum circuits. Because

$$\hat{H} - E_i = \frac{1 - \delta\tau(\hat{H} - E_i + 1/\delta\tau)}{\delta\tau} \simeq \frac{e^{-\delta\tau(\hat{H} - E_i + 1/\delta\tau)}}{\delta\tau}, \quad (\text{S1})$$

The Davidson generator can be obtained by using a energy shift of $E - 1/\delta\tau$ in the exponential operator. Define $\hat{H}'_i = \hat{H} - E_i + 1/\delta\tau$

$$|\Phi'\rangle = c^{1/2} e^{-\delta\tau\hat{H}'_i} |\Phi_i\rangle \simeq e^{-i\hat{A}\delta\tau} |\Phi_i\rangle. \quad (\text{S2})$$

where $\hat{A} = \sum_{\alpha} a_{\alpha} \hat{P}_{\alpha}$ and \hat{P}_{α} are the Pauli words. c is the normalization factor. The above mapping can be achieved by using the method developed in Ref. [55]. The coefficients a_I can be solved via the linear algebra $Sa = b$ where

$$S_{\alpha\beta} = \langle \Phi_I | \hat{P}_{\alpha}^{\dagger} \hat{P}_{\beta} | \Phi_I \rangle = \sum_{KL} V_{KI}^{*} V_{LI} \langle \Psi_K | \hat{P}_{\alpha}^{\dagger} \hat{P}_{\beta} | \Psi_L \rangle. \quad (\text{S3})$$

and

$$b_{\alpha} = -\frac{i}{\sqrt{c}} \Im[\langle \Phi_I | \hat{P}_{\alpha}^{\dagger} \hat{H}' | \Phi_I \rangle] \quad (\text{S4})$$

Algorithm S1 Classical Davidson algorithm for obtaining N_I lowest eigenvalues (and eigenvectors) of a matrix H with initial orthogonal guess vector $\{|b_I\rangle\}$ ($\langle b_I | b_J \rangle = \delta_{IJ}$).

-
- 1: **procedure** DAVIDSON($H, N_I, \{|b_I\rangle\}$)
 - 2: Form the subspace matrix $\bar{H} = \langle b_I | H | b_J \rangle$.
 - 3: Solve the subspace eigenvalue problem: $\bar{H}_{IJ} C_{JK} = C_{IK} h_K$.
 - 4: Obtain the N_I lowest eigenvalues h_K and the corresponding eigenvectors $|\Phi_I\rangle = \sum_K C_{KI} |b_K\rangle$.
 - 5: Form the residual vectors: $|r_I\rangle = (H - E_I) |\Phi_I\rangle$.
 - 6: Check the norm $\| |r_I\rangle \|$ of the residues for the convergence of each root $\text{norm}(r_I) \leq \epsilon$?
 - 7: **for** I in the non-converged roots **do**
 - 8: Form the pre-conditioned correction vector: $|\delta_I\rangle = -(\bar{H} - h_I)^{-1} |r_I\rangle$ and normalize.
 - 9: Orthogonalize to the current trial subspace: $|\delta'_I\rangle = |\delta_I\rangle - \sum_J |b_J\rangle \langle b_J | \delta_I \rangle / \langle b_J | b_J \rangle$.
 - 10: **if** $\text{norm}(|\delta'_I\rangle) / \text{norm}(|\delta_I\rangle) > \epsilon$ **then**
 - 11: Normalize $|\delta'_I\rangle$ and add it to the subspace.
 - 12: **end if**
 - 13: **end for**
 - 14: **end procedure**
-

C_2H_4	Basis set: STO-3G Hartree-Fock Energy: -77.0739546295 Hartree
	C 0.000000000 0.000000000 0.652999000 C 0.000000000 0.000000000 -0.652999000 H 0.000000000 0.915997000 1.229260000 H 0.000000000 -0.915997000 1.229260000 H 0.000000000 0.915997000 -1.229260000 H 0.000000000 -0.915997000 -1.229260000
$C_3H_3^+$	Basis set: STO-3G Hartree-Fock Energy: -113.620321176 Hartree
	C 0.000000000 0.794870000 0.000000000 C 0.688378000 -0.397435000 0.000000000 C -0.688378000 -0.397435000 0.000000000 H 1.636710000 -0.944955000 0.000000000 H 0.000000000 1.889910000 0.000000000 H -1.636710000 -0.944955000 0.000000000
C_6H_6	Basis set: STO-3G Hartree-Fock Energy: -227.891360223 Hartree
	C 0.000000000 1.386832000 0.000000000 C 1.201032000 0.693416000 0.000000000 C -1.201032000 0.693416000 0.000000000 C 1.201032000 -0.693416000 0.000000000 C -1.201032000 -0.693416000 0. C 0.000000000 -1.386832000 0.000000000 H 2.138466000 1.234644000 0.000000000 H -2.138466000 1.234644000 0.000000000 H 2.138466000 -1.234644000 0.000000000 H -2.138466000 -1.234644000 0.000000000 H 0.000000000 -2.469288000 0.000000000 H 0.000000000 2.469288000 0.000000000

TABLE S1. Cartesian coordinates of molecular systems that were used in this study.

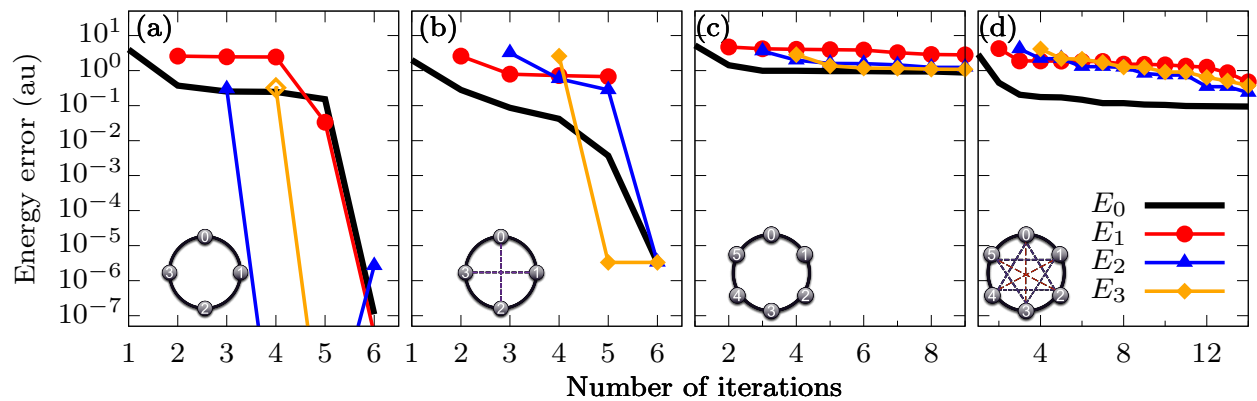


FIG. S1. Energy differences of the 1D Heisenberg models [55] as a function of QLancosz algorithm iteration. The energy difference is defined as $E_{algorithm} - E_{exact}$. Results for different states are given with different colors: black - ground state; blue - first excited state; green; second excited state; red - third excited state. Graphical representations of each system are given in the left bottom corner of each graph. The small circles with numbers represent spins, while lines connecting those circles represent $C_k \hat{S}_i \hat{S}_j$ terms. Different C_k coefficients are illustrated with lines of different colors and widths.

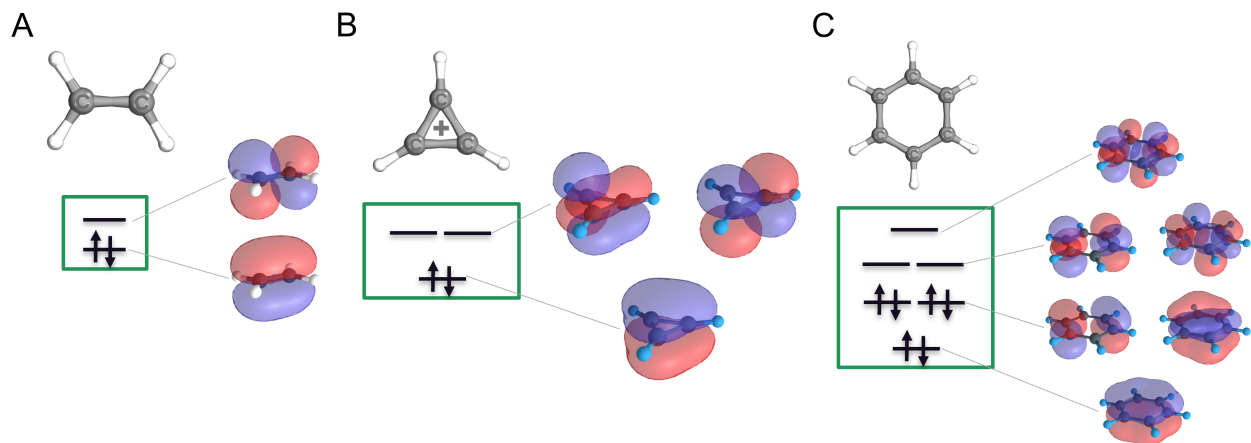


FIG. S2. Molecular orbitals chosen into an active space of investigated molecules: (A) ethylene; (B) cyclopropene cation; (C) benzene; (D) cyclooctatetraene dication.